

Neutrino oscillations in the presence of super-light sterile neutrinos.

P. C. Divari

*Department of Physical Sciences and Applications,
Hellenic Army Academy,
Vari 16673, Attica, Greece*

J. D. Vergados

*Theoretical Physics Division,
University of Ioannina,
Ioannina, GR 451 10, Greece*

(Dated: October 25, 2018)

In the present paper we study the effect of conversion of super-light sterile neutrino (SLSN) to electron neutrino in matter like that of the Earth. In the Sun the resonance conversion between SLSN and electron neutrino via the neutral current is suppressed due to the smallness of neutron number. On the other hand, neutron number density can play an important role in the Earth, making the scenario of SLSN quite interesting. Reactor neutrino experiments with medium baseline can help us to probe this scenario.

PACS numbers: 14.60.St, 13.35.Hb, 14.60.Pq, 26.65.+t, 13.15.+g

I. INTRODUCTION

Neutrinos are one of the most interesting constituents of particle physics. They interact only via the weak interaction and are nearly massless. In the standard picture, there are three neutrino species ν_1 , ν_2 and ν_3 , with a summed mass that solar and atmospheric oscillation observations bound to be above 0.06 eV (e.g. [1, 2]). Specifically, the neutrino oscillation depends on two mass splittings (Δm_{21}^2 and Δm_{31}^2), three mixing angles (θ_{12} , θ_{13} and θ_{23}) and a CP-violating Dirac phase, δ_D . In fact, the oscillation data show that the three ordinary active neutrinos ν_e , ν_μ and ν_τ are

mainly mixed with the three light neutrinos ν_1 , ν_2 and ν_3 with masses such that

$$\Delta m_{sol}^2 = \Delta m_{21}^2 \quad (1)$$

$$\Delta m_{atm}^2 = |\Delta m_{31}^2| \simeq |\Delta m_{32}^2| \quad (2)$$

with $\Delta m_{ij}^2 \equiv m_i^2 - m_j^2$. Δm_{atm}^2 and Δm_{sol}^2 stands for the atmospheric and the solar mass-squared splitting, respectively.

The neutrino mass hierarchy (or the ordering of the neutrino masses), i.e., whether the ν_3 neutrino mass eigenstate is heavier or lighter than the ν_1 and ν_2 mass eigenstates, is one of the remaining undetermined fundamental features of the neutrino Standard Model. The scenario, in which the ν_3 is heavier, is referred to as the normal mass hierarchy (NH). The other scenario, in which the ν_3 is lighter, is referred to as the inverted mass hierarchy (IH). The pattern of neutrino masses and mixings is schematically shown in Fig. 1. Most of the neutrino parameters entering neutrino

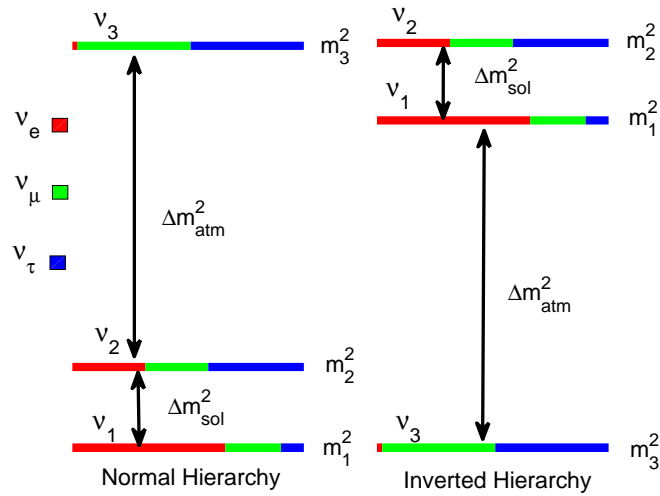


FIG. 1: (Color on line). Pattern of neutrino masses for the normal and inverted hierarchies is shown as mass squared. Flavor composition is indicated by the horizontal divisions (ν_e on the left, ν_μ in the middle, and ν_τ on the right). $\Delta m_{atm}^2 = |\Delta m_{31}^2| \simeq |\Delta m_{32}^2|$ and $\Delta m_{sol}^2 = \Delta m_{21}^2$ stands for the atmospheric and the solar mass-squared splitting, respectively.

oscillation formula are well determined except for the CP violating phase δ_D and the sign of $m_3^2 - m_1^2$ (the neutrino mass hierarchy pattern). From all the recent sensitivity studies it has clearly emerged that, at least for the next five years, it will be extremely

difficult for a single experiment to provide definitive information for any of the two searched properties CP-violation and neutrino-mass-hierarchy.

The neutrino sector may be richer than commonly believed and not confined to the 3-flavor framework. Several anomalies have recently emerged in short base line (SBL) oscillation experiments, which indicate significant extensions in the Standard picture and point towards the existence of new physics. The most famous examples are the $\nu_\mu \rightarrow \nu_e$ and/or $\bar{\nu}_\mu \rightarrow \bar{\nu}_e$ transitions in short baseline LSND and MiniBooNE experiments [3], reactor neutrino deficit [4] and Gallium anomaly [5, 6]. A recent careful analysis of neutrino anomaly (NA) [8–10] led to a challenging suggestion that there may be one or more additional eV scale massive sterile neutrinos [11–17]. One extra sterile neutrino is also suggested by recent analysis of the data from cosmological observations and Big-Bang Nucleosynthesis, in order to explain the existence of additional dark radiation in the Universe [18–24].

Furthermore, the large mixing angle (LMA) Mikheyev-Smirnov-Wolfenstein (MSW) solution [7, 25], to the solar neutrino problem, predicts an upturn of the energy spectrum of events at energies below 8 MeV. However, recent measurements of the energy spectra of the solar neutrino events at Super-Kamiokande-III [26], SNO [27], and Borexino [28] experiments do not show the expected (according to LMA) upturns at low energies. In [29, 30], a scenario is proposed to explain the suppression of the upturn. The scenario is based on the possible existence of a super-light sterile neutrino (SLSN) which weakly mixes with the active neutrinos. The new mass eigenstate is called ν_0 and its mass is denoted by m_0 . To explain the suppression of the upturn in the low energy solar data, it is shown that the mass squared difference with mass state ν_1 is around $\Delta m_{01}^2 \approx (0.7 - 2) \times 10^{-5} eV^2$ and the mixing angle with electron neutrino around $\sin^2 2\theta_{01} \approx (0.001 - 0.005)$ [29, 30]. Such a mixing leads to appearance of a dip in the ν_e - survival probability in the energy range (1 - 7) MeV, thus removing the upturn of the spectra. This is achieved with the help of a MSW resonant conversion of this SLSN with solar electron neutrino when neutrino travels from the interior of the Sun to the outside.

One of the major concerns in neutrino oscillation experiments is the effect of Earth matter in neutrino flavor conversion. One would naively expect that a similar reso-

nant flavor conversion between SLSN and electron neutrino should also happen when neutrinos propagate in Earth matter. In the Sun the neutron number density is small, thus the effect of neutral current interaction V_n can be effectively neglected. On the other hand, in Earth matter the neutron number density is of the same order of magnitude with electron number density [31–33]. Therefore, the effect of V_n can play an important role.

In the present paper, we present a comprehensive study of the dependence of SLSN transition probability on a sizeable potential of the neutral current interaction with matter. We consider a four-neutrino (4ν) scheme to calculate active-SLSN oscillations in matter, extending the study presented in Ref. [34] where it was assumed that the electron neutrino has non-negligible mixing only with the two massive neutrinos which generate the solar squared-mass difference. This paper is organized as follows. In Section II it is given the 4ν framework of neutrino evolution in Earth matter, adopting a simplified version of Earth reference model. In Section III we give numerical results for the conversion probability of electron neutrino to sterile one, in terms of mixing and mass splitting parameters. For the completeness of the discussion in this article we explore the capacity of a reactor experiment to probe the super-light sterile neutrino scenario. Conclusions are drawn in Sec. V.

II. FOUR NEUTRINO SCHEME

The four neutrino mixing matrix can be described by six mixing angles and three physical Dirac phases. If the neutrinos are of Majorana type, there will also be three Majorana CP-violating phases which do not show up in the neutrino oscillation patterns. Following the notation in [30], we call the mass eigenstates as $(\nu_0, \nu_1, \nu_2, \nu_3)$ with mass eigenvalues (m_0, m_1, m_2, m_3) . The flavor eigenstates are related to mass eigenstates by a 4×4 unitary matrix, U as follows

$$\begin{pmatrix} \nu_s \\ \nu_e \\ \nu_\mu \\ \nu_\tau \end{pmatrix} = U \cdot \begin{pmatrix} \nu_0 \\ \nu_1 \\ \nu_2 \\ \nu_3 \end{pmatrix} \quad (3)$$

The sterile neutrino, ν_s , is mainly present in the mass eigenstate ν_0 with mass m_0 . It mixes weakly with active neutrinos and this mixing can be treated as small perturbation of the standard LMA structure. The matrix U is a 4×4 unitary matrix describing the mixing of neutrinos. Neglecting CP violating phases, it can be parameterized by

$$U = R(\theta_{23})R(\theta_{13})R(\theta_{12})R(\theta_{02})R(\theta_{01})R(\theta_{03}), \quad (4)$$

where $R(\theta_{ij})$ is a 4×4 rotation matrix with a mixing angle θ_{ij} appearing at i and j entries, e.g.

$$R(\theta_{01}) = \begin{pmatrix} \cos \theta_{01} & \sin \theta_{01} & 0 & 0 \\ -\sin \theta_{01} & \cos \theta_{01} & 0 & 0 \\ 0 & 0 & 1 & 0 \\ 0 & 0 & 0 & 1 \end{pmatrix}, \quad R(\theta_{13}) = \begin{pmatrix} 1 & 0 & 0 & 0 \\ 0 & \cos \theta_{13} & 0 & \sin \theta_{13} \\ 0 & 0 & 1 & 0 \\ 0 & -\sin \theta_{13} & 0 & \cos \theta_{13} \end{pmatrix}, \quad (5)$$

$$R(\theta_{02}) = \begin{pmatrix} \cos \theta_{02} & 0 & \sin \theta_{02} & 0 \\ 0 & 1 & 0 & 0 \\ -\sin \theta_{02} & 0 & \cos \theta_{02} & 0 \\ 0 & 0 & 0 & 1 \end{pmatrix}, \quad R(\theta_{12}) = \begin{pmatrix} 1 & 0 & 0 & 0 \\ 0 & \cos \theta_{12} & \sin \theta_{12} & 0 \\ 0 & -\sin \theta_{12} & \cos \theta_{12} & 0 \\ 0 & 0 & 0 & 1 \end{pmatrix}, \quad (6)$$

and

$$R(\theta_{03}) = \begin{pmatrix} \cos \theta_{03} & 0 & 0 & \sin \theta_{03} \\ 0 & 1 & 0 & 0 \\ 0 & 0 & 1 & 0 \\ -\sin \theta_{03} & 0 & 0 & \cos \theta_{03} \end{pmatrix}, \quad R(\theta_{23}) = \begin{pmatrix} 1 & 0 & 0 & 0 \\ 0 & \cos \theta_{23} & \sin \theta_{23} & 0 \\ 0 & -\sin \theta_{23} & \cos \theta_{23} & 0 \\ 0 & 0 & 0 & 1 \end{pmatrix}. \quad (7)$$

$\theta_{12,13,23}$ are the mixing angles governing the flavor conversion of solar neutrinos, reactor neutrinos at short baseline and atmospheric neutrinos separately and they have been measured in solar, atmospheric, long baseline and reactor neutrino experiments [35–38].

The evolution of solar neutrinos propagating in Earth matter is described by the equation

$$i \frac{d\Psi}{dt} = (UH_0U^\dagger + \mathcal{V})\Psi \quad (8)$$

where $\Psi = (\psi_s, \psi_e, \psi_\mu, \psi_\tau)^T$ is the flavour transition amplitudes and

$$H_0 = \frac{1}{2E} \text{diag}\{\Delta m_{01}^2, 0, \Delta m_{21}^2, \Delta m_{31}^2\}$$

$$V = \text{diag}\{0, V_e + V_n, V_n, V_n\} \quad (9)$$

where E is the neutrino energy and $\Delta m_{kj}^2 = m_k^2 - m_j^2$. The charged-current and neutral-current matter potentials are defined as

$$V_e = \sqrt{2}G_F N_e \simeq 7.63 \times 10^{-14} \frac{N_e}{N_A} \text{ eV} \quad , \quad V_n = -\frac{1}{2}\sqrt{2}G_F N_n \quad , \quad (10)$$

where G_F is the Fermi constant, N_e is the electron number density, N_n is the neutron number density, and N_A is the Avogadro's number. All neutrino flavors interact with Earth matter constituents (electrons and neutrons) as they travel to the detection point (see Fig. 2). The charge-current neutrino matter potential used in this paper is taken from Ref. [32]. Since in the Earth the neutron number density is roughly of the same order of the electron number density, the neutral-current is taken to be $V_n = -0.5V_e$.

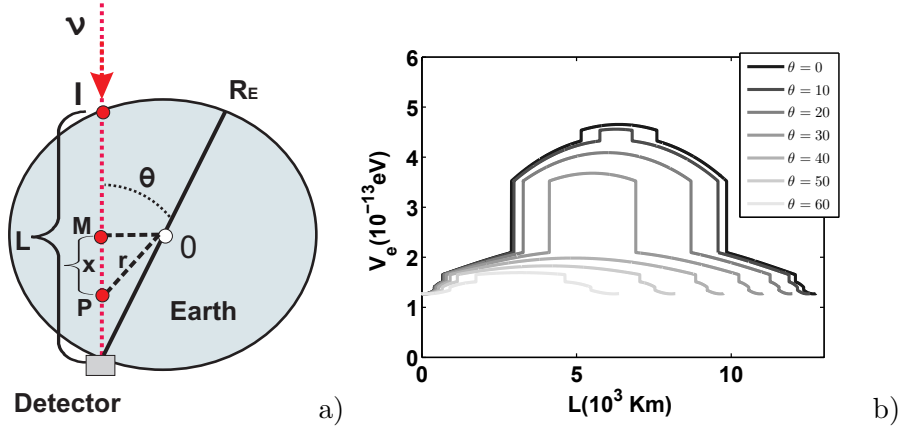


FIG. 2: (Color on line). Left panel: a schematic view of the solar neutrinos trajectories from the entry point (I) to the detector. θ is the nadir angle of the neutrinos. Right panel: The electron current matter potential V_e is shown as a function of neutrino travelling distance L for nadir angles $\theta = 0^\circ$ to $\theta = 60^\circ$. The data is based on the Preliminary Reference Earth Model (PREM) [32]. The Earth radius is taken $R_E = 6370 \text{ Km}$.

III. NUMERICAL RESULTS

In order to calculate the neutrino evolution inside the Earth matter, an accurate description of the Earth density profile is needed. For this reason a simplified version of the preliminary Earth reference model (PREM) [32] is employed, which contains five shells [33] and uses the polynomial function

$$N_{ei}(r) = (\alpha_i + \beta_i r^2 + \gamma_i r^4)N_A \quad (11)$$

for the i -th shell ($1 \leq i \leq 5$, where $i = 1$ is the innermost shell) to describe the Earth's electron density at the radial distance r (see Fig. 2(a)). The values of the coefficients are given in Table I for nadir angle $\theta = 0$. For nadir angles $\theta \neq 0$ Eq. (11) becomes

$$N_{ei}(r) = (\alpha'_i + \beta'_i x^2 + \gamma'_i x^4)N_A \quad (12)$$

where

$$\begin{aligned} \alpha'_i &= \alpha_i + \beta_i \sin^2\theta + \gamma_i \sin^4\theta \\ \beta'_i &= \beta_i + 2\gamma_i \sin^2\theta \\ \gamma'_i &= \gamma_i \end{aligned} \quad (13)$$

where x is the distance from the trajectory midpoint M to the generic position of the neutrino (see Fig. 2(a)).

Since, it is rather difficult to study equation Eq. (8) analytically, a numerical treatment based on the fourth-order Runge-Kutta method is used to solve the evolution equation of the neutrino states. Relevant neutrino parameters in this calculation are [35]

$$\Delta m_{21}^2 = (7.50 \pm 0.20) \times 10^{-5} \text{ eV}^2, \quad |\Delta m_{31}^2| = (2.32_{-0.08}^{+0.12}) \times 10^{-3} \text{ eV}^2, \quad (14)$$

$$\sin^2 2\theta_{12} = 0.857 \pm 0.024, \quad \sin^2 2\theta_{23} > 0.95. \quad (15)$$

After the discovery of a not small θ_{13} by Daya-Bay collaboration [36], confirmed by RENO experiment [37], a precise measurement of θ_{13} has been achieved by Daya-Bay experiment [38]:

$$\sin^2 2\theta_{13} = 0.089 \pm 0.010 \pm 0.005. \quad (16)$$

i	Shell	$[r_{i-1}, r_i]$	α_i	β_i	γ_i
1	Inner core	[0, 0.192]	6.099	-4.119	0.000
2	Outer core	[0.192, 0.546]	5.803	-3.653	-1.086
3	Lower mantle	[0.546, 0.895]	3.156	-1.459	0.280
4	Transition Zone	[0.895, 0.937]	-5.376	19.210	-12.520
5	Upper mantle	[0.937, 1]	11.540	-20.280	10.410

TABLE I: Descriptions of the simplified PREM model with five shells. The shell names and the values of the coefficients are quoted from Table 1 of Ref. [33] (see text for details). The radial distance r is normalized to the Earth radius R_E .

Recently, JUNO and RENO-50 long baseline reactor experiments, explore the capacity to probe the super light sterile neutrino scenario [39]. It is predicted that the bounds on $\sin^2 \theta_{01}$ and $\sin^2 \theta_{02}$ at $\Delta m_{01}^2 = 2 \times 10^{-5} \text{ eV}^2$, can be at best down to 2.8×10^{-3} and 4.2×10^{-3} , respectively. These values are laying inside the parameter range indicated in [29, 30] (*i.e.*, $\Delta m_{01}^2 = (0.7 - 2) \times 10^{-5} \text{ eV}^2$ and $\sin^2 \theta_{01}, \sin^2 \theta_{02} \sim 10^{-3}$). For intermediate baselines for which $\Delta m_{31}^2 L/E \sim \pi$, θ_{01} and θ_{02} parameters cannot be resolved. However, such experiments are sensitive to the parameter θ_{03} . The atmospheric data [40] and MINOS experiment [41] have already put the constrain

$$\sin^2 \theta_{03} < 0.2 \quad (17)$$

More stringent bounds are placing from cosmology. Recent PLANCK data constrain the effective number of relativistic species N_{eff} , before the big bang nucleosynthesis (BBN) epoch [42]. If θ_{03} or θ_{02} are large enough, ν_s can reach thermal equilibrium at the early universe and can be considered as an extra degree of freedom, contributing to $N_{eff} = 3.68_{-0.70}^{+0.80}$ [43]. From this observation, Ref. [44] puts stronger bounds

$$\sin^2 \theta_{01}, \sin^2 \theta_{02}, \sin^2 \theta_{03} < 10^{-3}$$

In the following analysis the dependence of mixing angle θ_{01} , θ_{02} and θ_{03} parameters as well as the splitting mass Δm_{01}^2 parameter on neutrino oscillations are investigated.

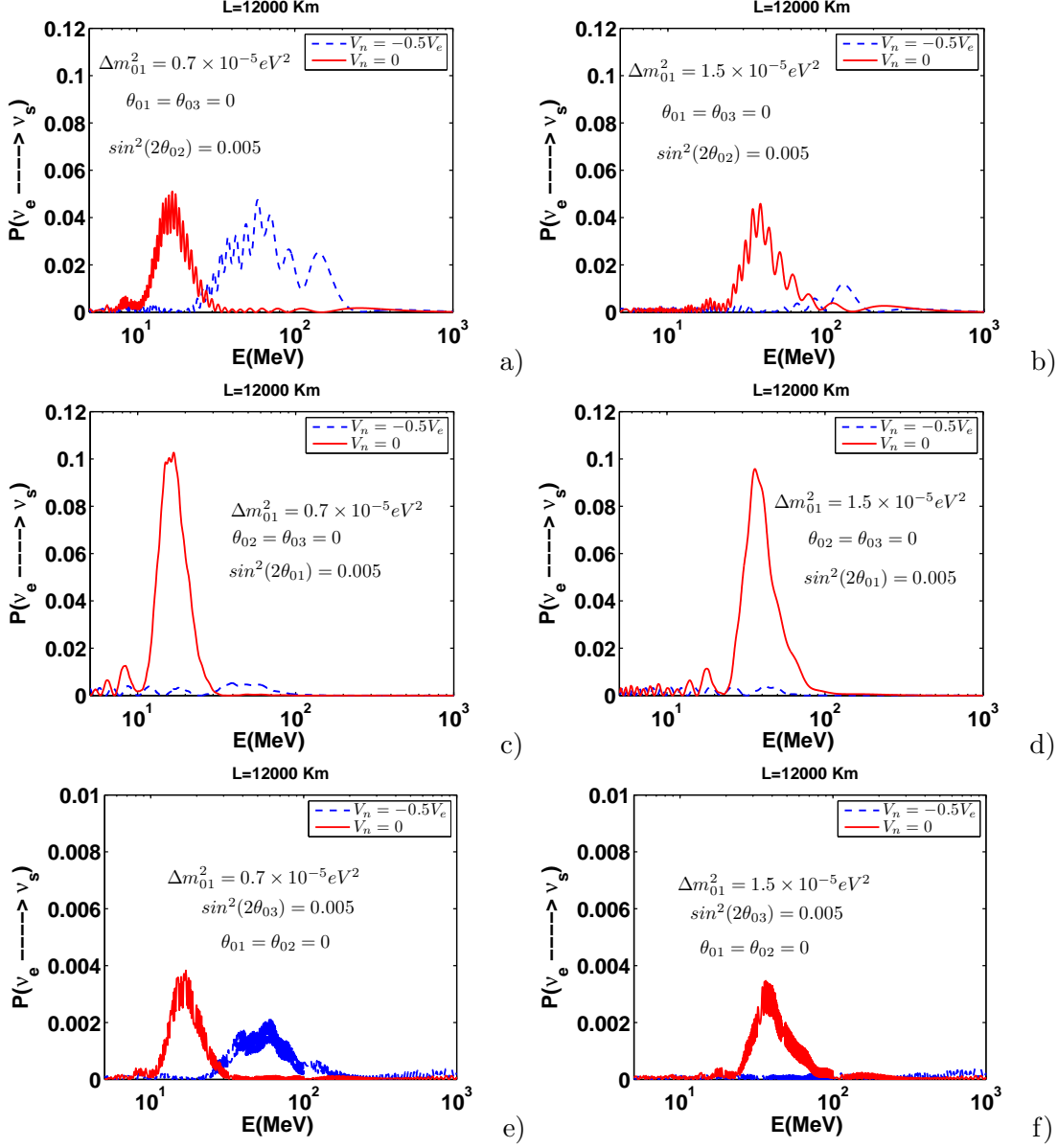


FIG. 3: (Color on line) Conversion probability $\nu_e \rightarrow \nu_s$ versus energy for $V_n = 0$ and for $V_n = -0.5V_e$ at fixed $L = 12000$ km.

Fig.3 depicts the conversion probability $\nu_e \rightarrow \nu_s$ in matter versus neutrino energy E , at fixed source-detector distance $L = 12000$ Km, for given neutrino masses and mixing angles [35–38]. By inspection of Fig.3 the following observations should be made: i) The resonant conversion probability $\nu_e \rightarrow \nu_s$ is much stronger when V_n is switched off ($V_n = 0$), and this happens at the energy around 17 MeV for $\Delta m_{01}^2 = 0.7 \times 10^{-5} \text{ eV}^2$, and around 37 MeV when Δm_{01}^2 becomes $1.5 \times 10^{-5} \text{ eV}^2$.

ii) The resonant conversion probability decreases for V_n included ($V_n = -0.5V_e$). iii) When V_n is taken into account, the maximal conversion probability, around 5%, happens for $\sin^2 2\theta_{02} = 0.005$, $\theta_{01} = \theta_{03} = 0$ with mass splitting $\Delta m_{01}^2 = 0.7 \times 10^{-5} \text{ eV}^2$ at energy around 60 MeV, which is well beyond the solar and supernovae neutrino spectrum. iv) In case where $\sin^2 2\theta_{03}$ has been involved, the conversion probability amplitude becomes much smaller, maximally around 0.2%. Ultimately, matter oscillations disappear for $\Delta m_{01}^2 = 1.5 \times 10^{-5} \text{ eV}^2$ (Fig. 3f). iv) As Δm_{01}^2 increases from $0.7 \times 10^{-5} \text{ eV}^2$ to $1.5 \times 10^{-5} \text{ eV}^2$, the conversion probability amplitude is strongly suppressed.

More details about the variation of the conversion probability $\nu_e \rightarrow \nu_s$ with respect to Δm_{01}^2 are given in Fig. 4. It is seen that as Δm_{01}^2 increases the amplitude of the conversion probability decreases. The decrease is more rapid when V_n included. Furthermore, the resonance position shifts to greater energies with greater mass splitting Δm_{01}^2 .

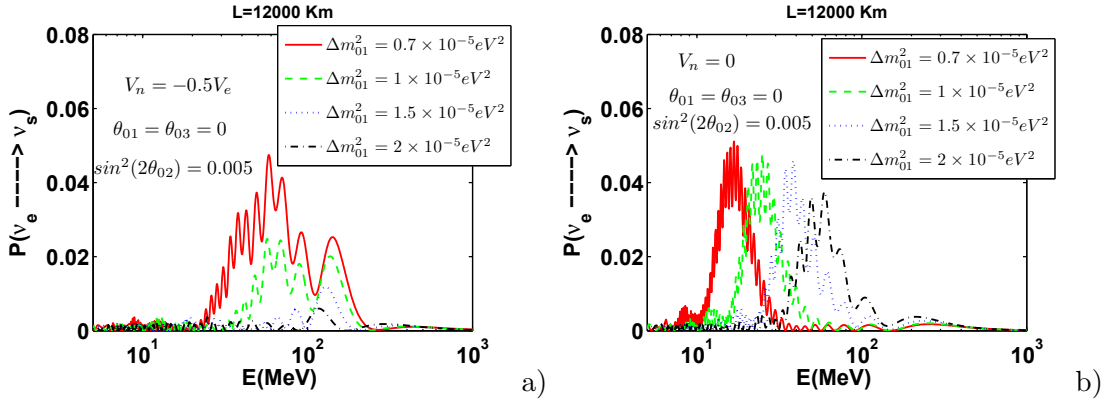


FIG. 4: (Color on line) (a) $\nu_e \rightarrow \nu_s$ conversion probabilities versus energy which correspond to cases with $\Delta m_{01}^2 = 0.7 \times 10^{-5} \text{ eV}^2$, $\Delta m_{01}^2 = 1.0 \times 10^{-5} \text{ eV}^2$, $\Delta m_{01}^2 = 1.5 \times 10^{-5} \text{ eV}^2$ and $\Delta m_{01}^2 = 2.0 \times 10^{-5} \text{ eV}^2$ separately. (a) $V_n = -0.5V_e$ (b) $V_n = 0$. $L = 12000 \text{ Km}$, $\theta_{01} = \theta_{03} = 0$ and $\sin^2 2\theta_{02} = 0.005$ for both cases.

It is also interesting to study the effect of V_n on the energy levels of neutrinos and on the resonant conversion probability $P(\nu_e \rightarrow \nu_s)$. In order to take into account the Earth matter effect, it is convenient to compute the energy levels of

$$H = UH_0U^\dagger + \mathcal{V} \quad (18)$$

taking a trajectory dependent averaged potential \bar{V}_e [45]

$$\bar{V}_e = \frac{1}{L} \int_0^L dx V_e(x) \quad (19)$$

where L is the length of the neutrino trajectory in the Earth. For baseline longer than 5000 km, \bar{V}_e varies from 1.36×10^{-13} eV to about 2.74×10^{-13} eV. For neutrinos crossing the core of the Earth (approximately $L = 12000$ Km), \bar{V}_e is found to be 2.74×10^{-13} eV. Figs. 5 and 6 show the eigenvalues E_0, E_1, E_2 and E_3 corresponding to neutrinos in the mass base ν_0, ν_1, ν_2 and ν_3 separately, as a function of the neutrino energy. We consider two different cases of Δm_{01}^2 . Also illustrated is the conversion probability amplitude $\nu_e \rightarrow \nu_s$ versus neutrino energy E for the two individual V_n values. We note that when a MSW resonance of flavor conversion takes place then two of the energy levels of the neutrino mass eigenstates ν_0 and ν_1 are getting close to each other. For $V_n = 0$ the two lines are crossing at a point with energy around 20 MeV for $\Delta m_{01}^2 = 0.7 \times 10^{-5}$ eV² and 60 MeV for $\Delta m_{01}^2 = 2 \times 10^{-5}$ eV², respectively. When $V_n = -0.5V_e$ (Fig. 6) the two energy lines are drifting apart and the resonance conversion probability has significantly suppressed. The absence of resonance is more clear as Δm_{01}^2 increases (Fig. 6(b)) where the resulting neutrino oscillations are getting more rapid.

Furthermore, Fig. 7 shows contour plots of $P(\nu_e, \nu_\mu, \nu_\tau \rightarrow \nu_s)$ as a function of neutrino energy E and nadir angle $\cos \theta$. The dark red area corresponds to maximal conversion probability $P(\nu_e, \nu_\mu, \nu_\tau \rightarrow \nu_s)$ and the dark blue to $P(\nu_e, \nu_\mu, \nu_\tau \rightarrow \nu_s) = 0$. For $\Delta m_{01}^2 = 0.7 \times 10^{-5}$ eV² (left panels) the maximal conversion probability (distinct red areas) occurs at lower energies (60-100) MeV and for nadir angles $\cos \theta \simeq (0.85 - 0.95)$, that is, for neutrinos travelling length approximately one Earth's diameter. As Δm_{01}^2 increases (right panels) a broadening region of both E and $\cos \theta$ is indicated (the distinct red areas are slightly dissolved). Moreover, the oscillation pattern moves to higher E , around (100-300)MeV, with oscillation amplitude being about three times smaller.

It should be mentioned that all the above discussion has been referred to the disappearance probability $P(\nu_{e,\mu,\tau} \rightarrow \nu_s)$ of active neutrinos from the sterile one. For the appearance probability $P(\nu_s \rightarrow \nu_{e,\mu,\tau})$ of active neutrinos from the sterile

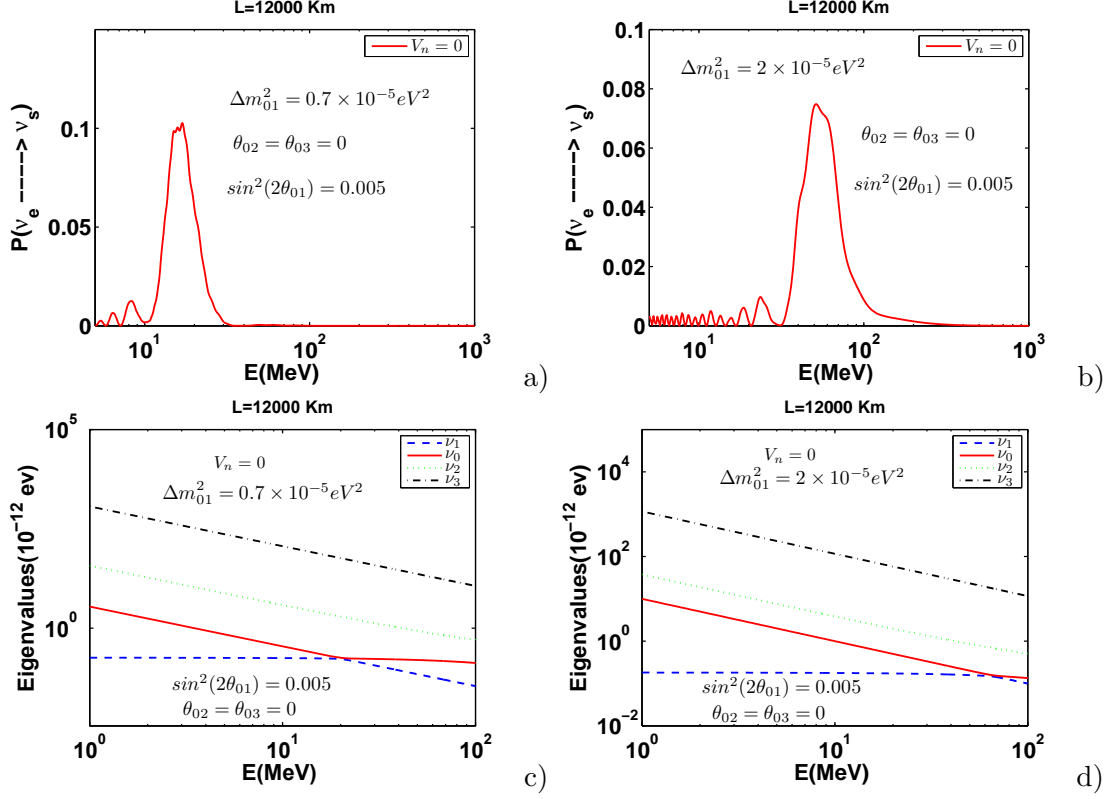


FIG. 5: (Color on line) Panels (a) and (b): $\nu_e \rightarrow \nu_s$ conversion probabilities versus neutrino energy E with $V_n = 0$. Panels (c) and (d): Eigenvalues of ν_0, ν_1, ν_2 and ν_3 versus neutrino energy E with $V_n = 0$. Two different cases of the parameter Δm_{01}^2 are considered at fixed $L = 12000\text{Km}$.

neutrino implies that $P(\nu_s \rightarrow \nu_{e,\mu,\tau}) = P(\nu_{e,\mu,\tau} \rightarrow \nu_s)$, since the CP violating phase in the mixing matrix U is not taken into account.

IV. SUPER LIGHT STERILE NEUTRINO OSCILLATION SEARCHES AT NUCLEAR REACTORS

Nuclear reactors are intense, isotropic sources of $\bar{\nu}_e$ produced by β -decay of fission fragments (i.e. U and Pu), into more stable nuclei: ${}^A_Z X \rightarrow {}^A_{Z-1} Y + e^- + \bar{\nu}_e$. The $\bar{\nu}_e$ energy is below 10 MeV, with an average value of ~ 3 MeV.

The neutrino oscillation search at a reactor (see Ref. [46] and references therein) is based on a disappearance measurement using the detection process $\bar{\nu}_e + p \rightarrow e^+ + n$.

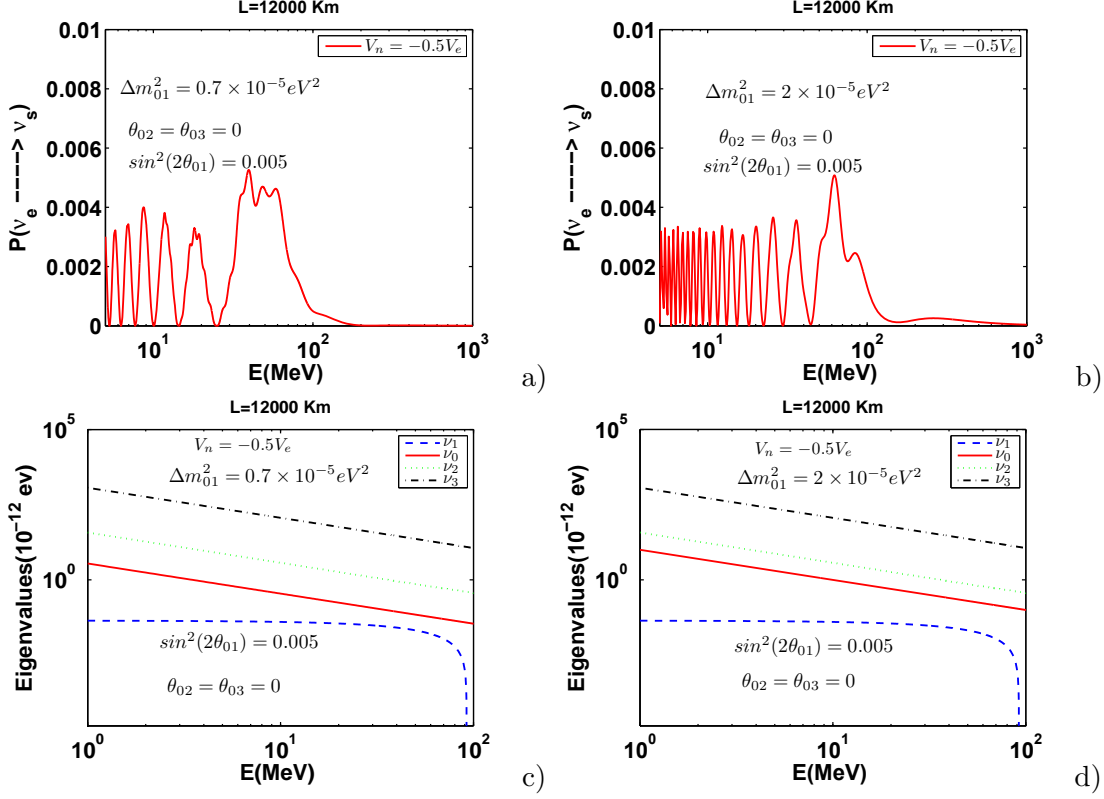


FIG. 6: (Color on line) Panels (a) and (b): $\nu_e \rightarrow \nu_s$ conversion probabilities versus neutrino energy E with $V_n = -0.5V_e$. Panels (c) and (d): Eigenvalues of ν_0, ν_1, ν_2 and ν_3 versus neutrino energy E with $V_n = -0.5V_e$. Two different cases of the parameter Δm_{01}^2 are considered. $L = 12000\text{Km}$.

It is widely accepted that a long-baseline disappearance reactor neutrino experiment, like those of JUNO and RENO-50 ($L \sim 50 \text{ km}$), with multiple detectors, could provide a clean measurement of the last undetermined neutrino mixing angle θ_{13} . Furthermore, these experiments could also be proposed for probing the super-light sterile neutrino scenario (SSNS).

Although the energy of the reactor neutrinos is of the order of a few MeV and the interaction cross section between matter and reactor antineutrinos is very tiny (10^{-44} cm^2), the huge emitted flux (210^{20} antineutrinos/second from a 1GW reactor) allows us to detect their signal. At such energies matter effects on the oscillation probability are negligible: $V_{eff} \sim G_F N_e \sim G_F N_n \ll \Delta m_{01}^2/E < \Delta m_{21}^2/E \ll |\Delta m_{31}^2/E|$. Thus

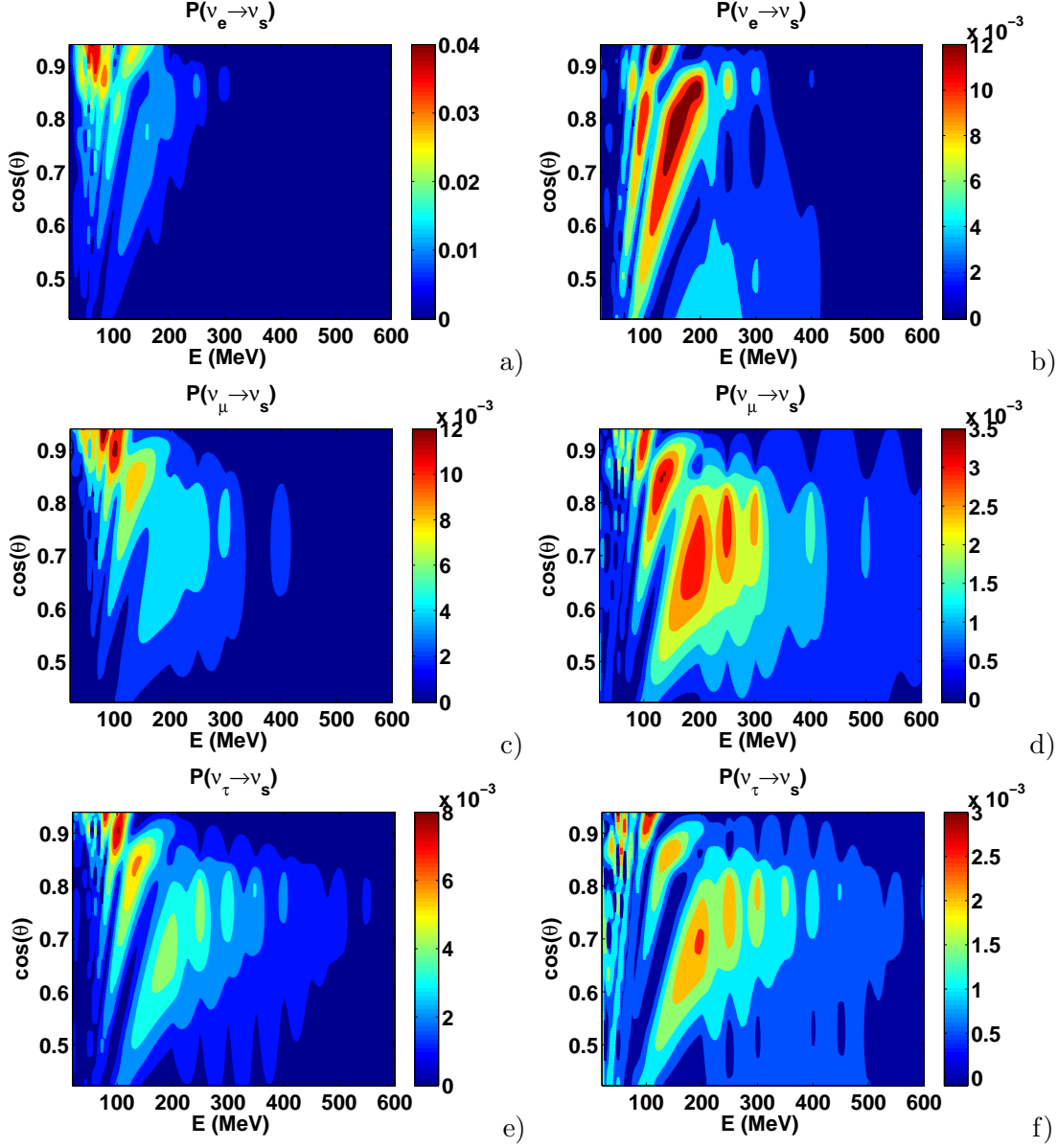


FIG. 7: (Color on line) Conversion probabilities as a function of nadir angle $\cos \theta$ (y-axis) and neutrino energy E (x-axis). The color represents the size of the conversion probability. The results are taken with $V_n = -0.5V_e$. The sterile neutrino mixing parameters are: $\theta_{01} = \theta_{03} = 0$ and $\sin^2 2\theta_{02} = 0.005$. $\Delta m_{01}^2 = 0.7 \times 10^{-5} \text{ eV}^2$ (left panels) and $\Delta m_{01}^2 = 1.5 \times 10^{-5} \text{ eV}^2$ (right panels).

the disappearance probability is given simply by

$$P(\bar{\nu}_e \rightarrow \bar{\nu}_e) = |M_0 e^{i\Delta_0} + M_1 e^{i\Delta_1} + M_2 e^{i\Delta_2} + M_3 e^{i\Delta_3}|^2 \quad (20)$$

where $\Delta_i = m_i^2 L / 2E$, $i = 0, 1, 2, 3$ and

$$\begin{aligned} M_0 &= |c_{03}(-c_{01}s_{12}c_{13}s_{02} - c_{13}s_{01}c_{12}) - e^{i\delta_D}s_{03}s_{13}|^2, \\ M_1 &= (c_{13}c_{12}c_{01} - c_{13}s_{12}s_{01}s_{02})^2 \\ M_2 &= (s_{12}c_{13}c_{02})^2 \\ M_3 &= |s_{03}c_{13}(-c_{12}s_{01} - c_{01}s_{02}s_{12}) + e^{i\delta_D}c_{03}s_{13}|^2. \end{aligned} \quad (21)$$

δ_D being the Dirac CP-violating phase and $c_{ij} = \cos \theta_{ij}$, $s_{ij} = \sin \theta_{ij}$, $c_{0i} = \cos \theta_{0i}$, $s_{0i} = \sin \theta_{0i}$ $i, j = 1, 2, 3$. In the absence of mixing with the sterile neutrinos, we recover the standard formula:

$$P(\bar{\nu}_e \rightarrow \bar{\nu}_e) = |\cos^2 \theta_{13} \cos^2 \theta_{12} e^{i\Delta_1} + \cos^2 \theta_{13} \sin^2 \theta_{12} e^{i\Delta_2} + \sin^2 \theta_{13} e^{i\Delta_3}|^2 \quad (22)$$

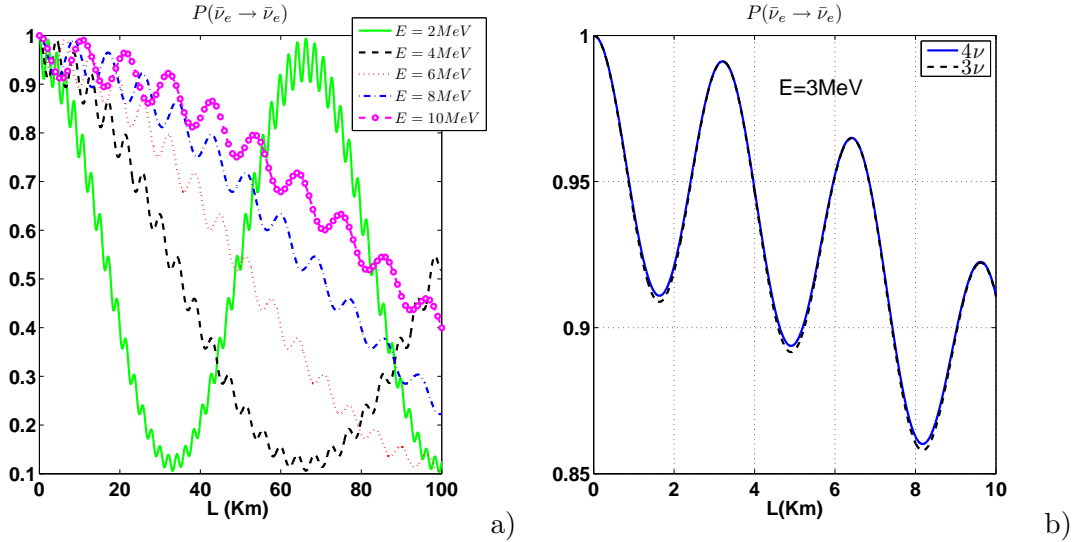


FIG. 8: (Color on line). (a): Oscillation pattern in $P(\bar{\nu}_e \rightarrow \bar{\nu}_e)$ disappearance probability as a function of baseline L , for various neutrino energies. (b): Disappearance probability $P(\bar{\nu}_e \rightarrow \bar{\nu}_e)$ as a function of L for neutrino energy $E = 3\text{MeV}$ in 4ν (blue solid) and 3ν (black dashed) mixing model. The following oscillation parameters were used in both panels: $\Delta m_{01}^2 = 2 \times 10^{-5} \text{eV}^2$, $\sin^2 2\theta_{01} = \sin^2 2\theta_{02} = \sin^2 2\theta_{03} = 0.005$.

TABLE II: Frequency and amplitude of the oscillatory term $4M_0M_i \sin^2(\Delta_{0i}L/E)$ entering Eq. (23).

Case	mixing angles	amplitude ($4M_0M_i$)	frequency (Δ_{0i})
I (i=1)	$\theta_{02} = \theta_{03} = 0$ and $\theta_{01} \neq 0$	$c_{13}^4 c_{12}^4 \sin^2 2\theta_{01}$	Δ_{01}
II (i=2)	$\theta_{01} = \theta_{03} = 0$ and $\theta_{02} \neq 0$	$s_{12}^4 c_{13}^4 \sin^2 2\theta_{02}$	$\Delta_{02} = \Delta_{21} - \Delta_{01}$
III (i=3)	$\theta_{01} = \theta_{02} = 0$ and $\theta_{03} \neq 0$	$s_{13}^4 \sin^2 2\theta_{03}$	$\Delta_{03} = \Delta_{31} - \Delta_{01}$

Figure 8(a) shows, the results of the disappearance probability $P(\bar{\nu}_e \rightarrow \bar{\nu}_e)$ as a function of baseline L for various neutrino energies E . It is worth noting that the oscillation probability $P(\bar{\nu}_e \rightarrow \bar{\nu}_e)$ beats because the frequency of the waves in (20) with $|\Delta m_{13}^2|$ differs from the frequencies associated with $|\Delta m_{12}^2|$ and $|\Delta m_{01}^2|$, which are smaller by a factor of 30 and 100 respectively compared to $|\Delta m_{13}^2|$ scale. The superposed waves can be decomposed into the beating low frequency wave and the high frequency wiggles within the beat. The frequency of wiggles is higher for smaller neutrino energies while the ratio of the period P of the wiggles to neutrino energy E , is $P/E \simeq 1$. We also note that at low E the oscillation wiggles grow smaller with higher baseline L . Moreover, the lower E is the more rapid the wiggles are in L , while as the neutrino energy E increases wiggling formation is diminishing.

The difference between the 4ν neutrino scheme (three active neutrinos and one sterile neutrino) over the conventional model with three active neutrinos is depicted in Fig. 8(b). As it is seen the difference (about 0.2%) between 4ν and 3ν models is evident at locations where $P(\bar{\nu}_e \rightarrow \bar{\nu}_e)$ exhibits minima. Therefore, the sterile neutrino can be detected only in a narrow region of L/E (about 0.25 Km/MeV) around the minimum points of $P(\bar{\nu}_e \rightarrow \bar{\nu}_e)$.

Let us now discuss the effects of each mixing by the sterile neutrino. In this case where one of the sterile mixing parameter is nonzero, the oscillation probability $P(\bar{\nu}_e \rightarrow \bar{\nu}_e)$ reduces into the form

$$P(\bar{\nu}_e \rightarrow \bar{\nu}_e) = 1 - 4 \sum_{i < j=0}^3 M_i M_j \sin^2 \left(\Delta_{ij} \frac{L}{E} \right) \quad (23)$$

where $\Delta_{ij} = (m_j^2 - m_i^2)/4$. By measuring the amplitudes ($4M_0M_i$) of the corresponding oscillatory modes $Y_i = 4M_0M_i \sin^2(\Delta_{0i}L/E)$, $i=1,2,3$, entering Eq. (23), the mixing parameters θ_{0i} can be determined. The mass splitting parameter Δm_{01}^2 can be extracted from the measured value of frequency. In Table II the amplitude and the frequency of the corresponding to one nonzero mixing parameter θ_{0i} oscillatory mode are listed.

Figure 9 displays, the oscillatory modes $Y_i = 4M_0M_i \sin^2(\Delta_{0i}L/E)$ as function of baseline L for three different reactor neutrino energies $E = 2, 4$ and 6MeV . Panel (a) depicts the oscillatory mode $Y_1 = 4M_0M_1 \sin^2(\Delta_{01}L/E)$ (case I of Table II). By measuring the frequency and amplitude of this oscillatory mode, the values of $\sin^2 2\theta_{01}$ and Δm_{01}^2 can be determined. Notice that to derive these values the detector has to be at distances of the order of 200-300 Km from the source. This basically defines a long-baseline experiment where the region probed extends to low values of Δm_{01}^2 but their reach in $\sin^2 2\theta_{01}$ is limited. As expected in the $\Delta m_{01}^2 \rightarrow 0$ limit, the sensitivity to $\sin^2 2\theta_{01}$ is lost. Similarly, in Fig.9 (b) and (c) the cases II and III of Table II are delineating. As it is seen, the mixing parameter θ_{03} can be determined in a baseline less than 10 Km, therefore experimental setups with longer baselines have no advantage. In case II and III the sensitivity of both $\sin^2 2\theta_{02}$ and $\sin^2 2\theta_{03}$ persists in the limit $\Delta m_{01}^2 \rightarrow 0$.

In all the above cases, the CP-violating phase δ_D do not appear in $P(\bar{\nu}_e \rightarrow \bar{\nu}_e)$, so had we set δ_D equal to some other value, the results would not have changed. However, when two or more mixing angles are nonzero, the Dirac CP-violating phases show up in $P(\bar{\nu}_e \rightarrow \bar{\nu}_e)$. In the present work we have taken the phase $\delta_D = 0$, i.e., assumed CP conservation. We have also assumed the ordering of the mass eigenstates to be normal.

The allowed regions in the $\sin^2 2\theta_{0i} - \Delta m_{01}^2$, $i=1,2,3$ planes can be determined with good precision and sufficient energy resolution by global fits to available neutrino oscillation data. These regions are relevant, for $\bar{\nu}_\mu \rightarrow \bar{\nu}_e$ appearance and $\bar{\nu}_e$ -disappearance searches. Marginal-allowed intervals of these oscillation parameters can be obtained by global fits to long or medium-baseline $\bar{\nu}_e$ -disappearance data (see e.g. Ref. [39]).

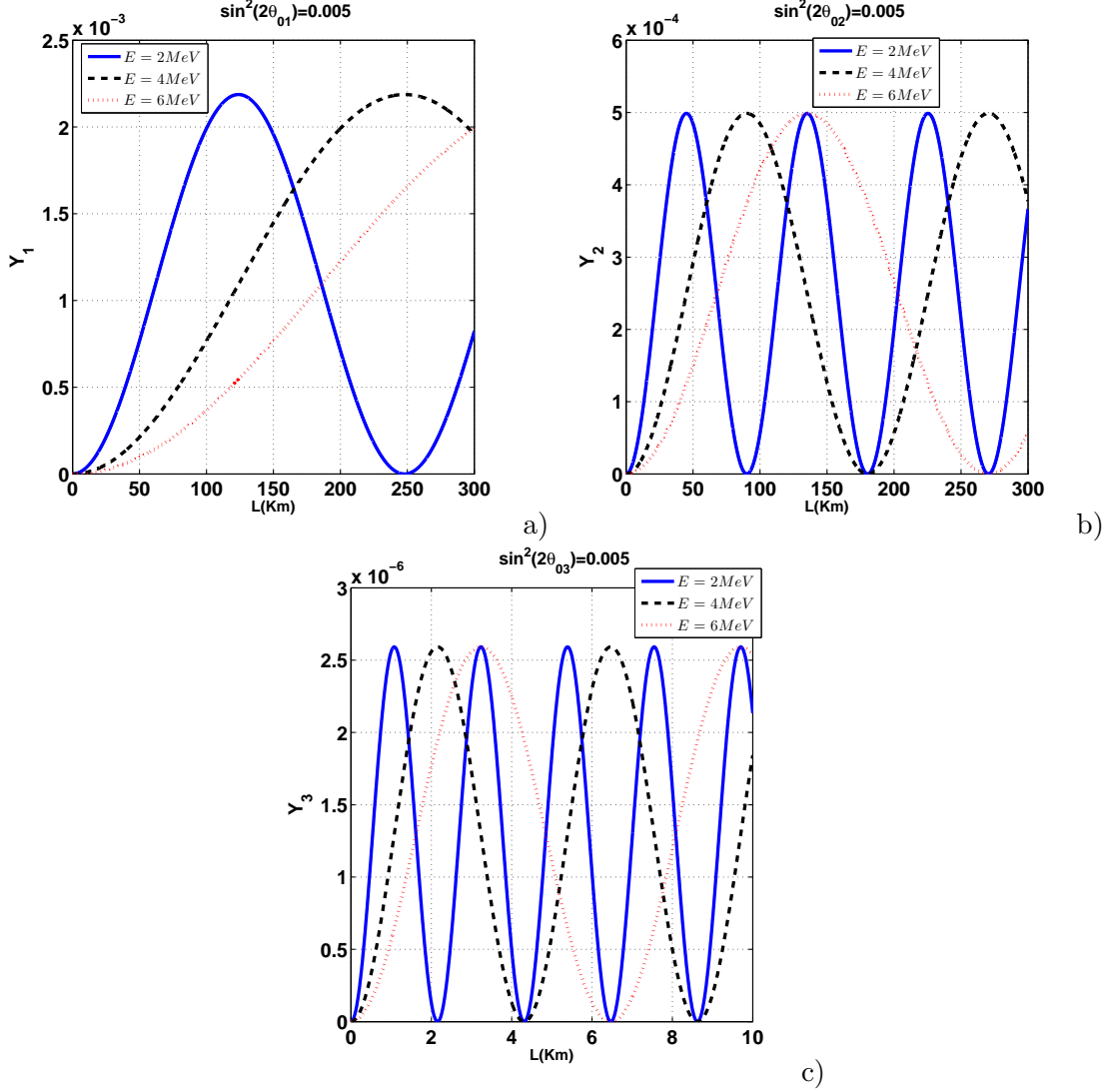


FIG. 9: (Color on line). Oscillatory modes $Y_i = 4M_0M_i \sin^2(\Delta_{0i}L/E)$ as function of L . The mass splitting parameter is taken $\Delta m_{01}^2 = 2 \times 10^{-5} \text{ eV}^2$. The sterile mixing parameters are: $\theta_{02} = \theta_{03} = 0$ and $\sin^2 2\theta_{01} = 0.005$ (a), $\theta_{01} = \theta_{03} = 0$ and $\sin^2 2\theta_{02} = 0.005$ (b) and $\theta_{01} = \theta_{02} = 0$ and $\sin^2 2\theta_{03} = 0.005$ (c).

V. CONCLUSIONS

Recent measurements of the energy spectra of the solar neutrino events at SuperKamiokande, SNO and Borexino do not show the expected (according to LMA) upturns at low energies. The absence of the upturn can be explained by mixing of very light sterile neutrino in the mass states $\nu_0, \nu_1, \nu_2, \nu_3$ with mass-squared differ-

ence $\Delta m_{01}^2 \approx (0.7 - 2) \times 10^{-5} \text{ eV}^2$ and mixing angles $\sin^2 2\theta_{0i} < 10^{-3}$, $i = 1, 2, 3$. Furthermore, cosmological data, mainly from observations of the cosmic microwave background and large scale structure suggest, the existence of a fourth degree-of-freedom ($N_f > 3$) which might be a sterile neutrino.

If SLSN exists it could oscillate with active neutrinos over the distance of the Earth's radius. A numerical treatment based on the fourth-order Runge-Kutta method is used to solve the evolution equation for matter corrections to oscillations of four neutrinos, adopting a simplified version of the preliminary Earth reference model.

Taking the neutral-current matter potential V_n to be -0.5 of the corresponding charge-current V_e , we found a resonant conversion at low energies around 17 MeV for $\Delta m_{01}^2 = 0.7 \times 10^{-5} \text{ eV}^2$ and around 37 MeV for $\Delta m_{01}^2 = 1.5 \times 10^{-5} \text{ eV}^2$ (neutrino path length $L \approx 12000 \text{ Km}$). This resonant conversion is much stronger when $V_n = 0$ and becomes much smaller when V_n is taken into account. Furthermore, when V_n included the resonance position is shifted to higher energies around 60 MeV. The above results are sensitive to mass-squared difference Δm_{01}^2 as well as to the mixing angle θ_{03} . It is found that as Δm_{01}^2 increases the conversion probability amplitude is strongly suppressed (0.2% for $\sin^2 2\theta_{03} = 0.005$) with oscillation pattern to occur in a broadening energy-nadir angle regions.

It is interesting to investigate the super light sterile neutrino scenario in a medium reactor antineutrino experiment. Since matter effects in a detector are negligible, the four-neutrino oscillations are based on vacuum-oscillation solution. It is worth noticing that the $\bar{\nu}_e$ disappearance exhibits high frequency wiggles in baseline L which grow smaller as L increases. The ratio of the wiggling period to the neutrino energy remains constant. Furthermore, we have shown that any information on sterile mixing angles $\theta_{01}, \theta_{02}, \theta_{03}$ comes from the oscillating modes with oscillation length larger than 10 Km. Therefore, unlike the case of $\text{sign}(\Delta m_{31}^2)$, farther sources at distances of the order of 200-300 Km could be crucial for improving the sensitivity to SLSN.

Nuclear reactors will continue to help us uncover more features about neutrinos. By enlarging the detector size and/or having more numerous and powerful sources and/or prolonging the data taking period, the sensitivity to SLSN can be increased to a

desired level. In the next 20 years, the upcoming next generation reactor experiments will tell us whether or not super-light sterile neutrinos exist.

VI. REFERENCES

- [1] M. Gonzalez-Garcia, M. Maltoni, J. Salvado, and T. Schwetz, JHEP 1212, 123 (2012).
- [2] K. Scholberg, Journal of Physics: Conference Series 312, 072002 (2011).
- [3] A. Aguilar-Arevalo et al. [LSND Collaboration], Phys. Rev. D 64 (2001) 112007; A. A. Aguilar-Arevalo et al. [MiniBooNE Collaboration], Phys. Rev. Lett. 110 (2013) 161801; T. Katori and J. M. Conrad, Advances in High Energy Physics Vol. 2015, Article ID 362971.
- [4] T. A. Mueller, D. Lhuillier, M. Fallot, A. Letourneau, S. Cormon, M. Fechner, L. Giot and T. Lasserre et al., Phys. Rev. C83, 054615 (2011).
- [5] J. N. Abdurashitov, V. N. Gavrin, S. V. Girin, V. V. Gorbachev, P. P. Gurkina, T. V. Ibragimova, A. V. Kalikhov and N. G. Khairnasov et al., Phys. Rev. C73, 045805 (2006).
- [6] J. Kopp, P. A. N. Machado, M. Maltoni and T. Schwetz, JHEP 1305, 050 (2013).
- [7] L. Wolfenstein, Phys. Rev. D17, 2369 (1978).
- [8] C. Giunti and M. Laveder, Phys. Rev. D82, 053005 (2010).
- [9] G. Mention et al., Phys. Rev. D 83, 073006 (2011).
- [10] J. Kopp, M. Maltoni and T. Schwetz, Phys. Rev. Lett. 107, 091801 (2011).
- [11] C. Giunti, M. Laveder, Y.F. Li and H.W. Long, Phys. Rev. D 88, 073008 (2013).
- [12] C. Giunti, M. Laveder, Y. Li, Q. Liu, and H. Long, Phys. Rev. D86, 113014 (2012).
- [13] C. Giunti and M. Laveder, Phys.Rev. D84, 093006 (2011).
- [14] C. Giunti and M. Laveder, Phys. Lett. B706, 200 (2011).
- [15] J. Conrad, C. Ignarra, G. Karagiorgi, M. Shaevitz, and J. Spitz, Advances in High Energy Physics Vol. 2013, Article ID 163897.
- [16] C. Giunti, M. Laveder, Y. Li, and H. Long, Phys. Rev. D87, 013004 (2013).
- [17] M. Archidiacono, N. Fornengo, C. Giunti, S. Hannestad, and A. Melchiorri, Phys.Rev. D87, 125034 (2013).
- [18] J. Hamann et al., Phys. Rev. Lett. 105, 181301 (2010); E. Giusarma et al., Phys. Rev.

- D 83, 115023 (2011); A.X. Gonzalez-Morales et al., arXiv:1106.5052 [astro-ph.CO]; J. Hamann, JCAP 1203, 021 (2012).
- [19] M. Archidiacono et al., Phys. Rev. D 86, 065028 (2012).
- [20] G. Mangano and P.D. Serpico, Phys. Lett. B 701, 296 (2011); J. Hamann et al., JCAP 1109, 034 (2011); T.D. Jacques, L.M. Krauss and C. Lunardini, Phys. Rev. D 87, 083515 (2013).
- [21] A. G. Riess, L. Macri, S. Casertano, H. Lampeitl, H. C. Ferguson, A. V. Filippenko, S. W. Jha and W. Li et al., Astrophys. J. 730, 119 (2011) [Erratum-ibid. 732, 129 (2011)].
- [22] A. Kusenko Phys. Rep. 481, 128 (2009).
- [23] M. Wyman, D. H.Rudd, R. A. Vanderveld and W. Hu, Phys. Rev. Lett. 112, 051302 (2014).
- [24] R. A. Battye and A. Moss, Phys. Rev.Lett. 112, 051303 (2014).
- [25] S. P. Mikheyev and A. Yu. Smirnov, Sov. J. Nucl. Phys. 42 (1985) 913; Nuovo Cim. C9, 17 (1986); Zh. Eksp. Teor. Fiz. 91, 7 (1986), [Sov. Phys. JETP 64, 4 (1986)].
- [26] SUPER-KAMIOKANDE collaboration, K. Abe et al., Phys. Rev. D83, 052010 (2011).
- [27] SNO Collaboration, B. Aharmim et al., Phys. Rev. C81, 055504 (2010).
- [28] The Borexino Collaboration, G. Bellini et al., Phys. Rev. D82, 03300 (2010).
- [29] P. C. de Holanda and A. Yu. Smirnov, Phys. Rev. D69, 113002 (2004)
- [30] P. C. de Holanda and A. Yu. Smirnov, Phys. Rev. D83, 113011 (2011).
- [31] C. W. Kim, A. Pevsner. *Neutrinos in Physics and Astrophysics*, Hardwood, (1995).
- [32] A.M. Dziewonski, D.L. Anderson, Physics of the Earth and Planetary Interiors, 25, 297 (1981).
- [33] E. Lisi, D. Montanino, Phys. Rev. D 56, 1792 (1997).
- [34] W. Liao, Y. Luo and X. Wu, JHEP 06, 069 (2014).
- [35] J. Beringer et al. [Particle group collaboration] Phys. Rev. D 86, 010001 (2012).
- [36] F. P. An et al. [Daya Bay collaboration], Phys. Rev. Lett. 108, 171803 (2012).
- [37] J. K. Ahn et al. [RENO collaboration], Phys. Rev. Lett. 108, 191802 (2012).
- [38] F. P. An et al. [Daya Bay collaboration], Chinese Phys. C 37, 011001 (2013).
- [39] P. Bakhti and Y. Farzan, JHEP 1310, 200 (2013).
- [40] M. Cirelli, G. Marandella, A. Strumia and F. Vissani, Nucl. Phys. B 708, 215 (2005).

- [41] P. Adamson *et al.* [MINOS Collaboration], Phys. Rev. D 81, 052004 (2010).
- [42] P. A. R. Ade *et al.* [Planck Collaboration], Astronomy and Astrophysics, 571, A16 (2014).
- [43] Y. I. Izotov and T. X. Thuan, Astrophys. J. 710, L67 (2010).
- [44] Mirizzi *et. al.*, Phys. Lett. B 726, 8014 (2013).
- [45] W. Liao, Phys. Rev. D 77, 053002 (2008).
- [46] P. Vogel, L. J. Wen and C. Zhang, Nature Communications 2015, DOI: 10.1038/ncomms7935